

Formation and Survival of Complex Organic Molecules in the Jovian Circumplanetary Disk

OLIVIER MOUSIS,¹ CLÉMENT PETETIN,² TOM BENEST COUZINOU,³ ANTOINE SCHNEEBERGER,⁴ AND YANNIS BENNACER³

¹*Solar System Science and Exploration Division, Southwest Research Institute, 1301 Walnut St, Ste 400, Boulder, CO, USA*

²*Groupe de Spectrométrie Moléculaire et Atmosphérique (GSMA), Université de Reims Champagne-Ardenne, CNRS, 51687 Reims cedex, France*

³*Aix-Marseille Université, CNRS, CNES, Institut Origines, LAM, Marseille, France*

⁴*Astronomy & Astrophysics Section, School of Cosmic Physics, Dublin Institute for Advanced Studies, 31 Fitzwilliam Place, Dublin D02 XF86, Ireland*

ABSTRACT

Europa, Ganymede, and Callisto are key targets in the search for habitability due to the potential presence of subsurface oceans. Detecting complex organic molecules (COMs), essential for prebiotic chemistry, is crucial to assessing their potential. Though COMs remain undetected on these moons, ESA’s JUICE and NASA’s Europa Clipper missions aim to fill this gap with their science payloads. This study explores the formation and transport of COMs within Jupiter’s circumplanetary disk (CPD), a critical environment for the formation of the Galilean moons. Using a time-dependent model that couples the evolving CPD structure with the dynamics of icy particles of varying sizes and release times, we assess two primary COM formation pathways: thermal processing of ices and UV photochemistry. The results indicate that heating, particularly of NH₃:CO₂ ices, occurs efficiently before substantial irradiation, making it the dominant pathway for COM formation in the Jovian CPD. However, the relative efficiencies of these two processes are governed by particle density, disk viscosity, accretion rate, and UV flux, which collectively determine drift timescales and exposure to favorable thermodynamic environments. Existing models indicate that Europa’s accretion was relatively cold and prolonged, possibly allowing some COMs to survive incorporation, whereas Ganymede and Callisto likely formed under even cooler conditions conducive to preserving COM-rich material. These results highlight the potential inheritance of complex organics by the Galilean moons and offer a framework for interpreting upcoming compositional data from JUICE and Europa Clipper.

Keywords: Solar system gas giant planets (1191) — Protoplanetary disks (1300) — Planet formation (1241) — Solar system formation (1530)

1. INTRODUCTION

Europa, Ganymede, and Callisto are believed to have subsurface oceans beneath their icy crusts (Kivelson et al. 2000), positioning them as key targets in the search for habitable environments within the Solar System (Grasset et al. 2013; Saur et al. 2015; Vance et al. 2023). It is critical to constrain the internal composition of these moons, particularly the presence of complex organic molecules (COMs), which are composed of carbon, hydrogen, oxygen, and often nitrogen, in order to evaluate their potential habitability. COMs are funda-

mental precursors to biomolecules, such as amino acids and nucleobases, that play a key role in prebiotic chemistry. The presence of COMs indicates ongoing organic chemical processes and suggests that these moons may contain the essential ingredients for life: liquid water, energy sources, and organic compounds (McKay et al. 2008; Hand et al. 2009).

There is still a lack of direct evidence for COMs in Europa, Ganymede, and Callisto. However, the upcoming ESA Jupiter Icy Moons Explorer (JUICE) (Grasset et al. 2013) and NASA Europa Clipper missions (Becker et al. 2024; Pappalardo et al. 2024) are likely to address this gap. Both missions will carry advanced instruments, including infrared spectrometers, submillimeter sensors, and mass spectrometers. These instru-

ments are designed to analyze the surface and exospheric compositions of these icy moons with unparalleled precision (Wurz et al. 2018; Hartogh 2023; Waite et al. 2024; Poulet et al. 2024). These observations are expected to provide valuable information about the chemical environments of the moons, including the presence and distribution of complex organic compounds, salts, and volatile ices. All of these are key indicators of potential habitability.

The formation and transport of COMs in protoplanetary disks (PPDs) have been extensively investigated (Walsh et al. 2014; Benest Couzinou et al. 2024, 2025). In contrast, comparatively little attention has been devoted to the synthesis, alteration, or survival of COMs within circumplanetary disks (CPDs), despite these being the environments in which the satellites of gas giants are thought to form (Canup & Ward 2002, 2006; Ronnet et al. 2017; Anderson et al. 2021). Although COMs can form efficiently in the protosolar nebula (PSN), their delivery to the forming Galilean moons is severely constrained. Inward transport toward Jupiter's orbit is inefficient and strongly size-dependent, while gap formation, irradiation, and thermal processing during transfer to the CPD likely destroy or chemically alter a large fraction of COMs. Consequently, only a limited fraction of PSN-formed COMs is expected to survive and be incorporated into moon-forming material (Couzinou et al. 2025). By comparison, the physical and chemical conditions in CPDs differ markedly from those in PPDs, opening the possibility of distinct chemical pathways. While elevated temperatures in CPDs can further degrade COMs inherited from the PPD, they may also promote in situ chemical processing of icy particles delivered from the PPD, enabling the formation of new COMs directly within the CPD.

The formation and transport of COMs in protoplanetary disks (PPDs) have been extensively investigated (Walsh et al. 2014; Benest Couzinou et al. 2024, 2025). In contrast, comparatively little attention has been devoted to the synthesis, alteration, or survival of COMs within circumplanetary disks (CPDs), despite these being the environments in which the satellites of gas giants are thought to form (Canup & Ward 2002, 2006; Ronnet et al. 2017; Anderson et al. 2021). Although COMs can form efficiently in the protosolar nebula (PSN), their delivery to the forming Galilean moons is severely constrained. Inward transport toward Jupiter's orbit is inefficient and strongly size-dependent, while gap formation, irradiation, and thermal processing during transfer to the CPD likely destroy or chemically alter a large fraction of COMs. Consequently, only a limited fraction of PSN-formed COMs is expected to survive and

be incorporated into moon-forming material (Couzinou et al. 2025). By comparison, the physical and chemical conditions in CPDs differ markedly from those in PPDs, opening the possibility of distinct chemical pathways. While elevated temperatures in CPDs can further degrade COMs inherited from the PPD, they may also promote in situ chemical processing of icy particles delivered from the PPD, enabling the formation of new COMs directly within the CPD.

In this study, we investigate the formation and transport of COMs within a CPD, using the model developed by Schneeberger & Mousis (2024), in which the accretion rate reflects the final stages of Jupiter's growth. This scenario leads the CPD to evolve from a hot to a cold state, encompassing a broad spectrum of thermodynamic conditions. We employ a time-dependent model that couples the evolving disk structure with the dynamics of icy particles of various sizes, released at different stages of the evolution of the CPD. We explore two COM formation pathways, both of which are grounded in laboratory experiments: (1) the thermal processing of ices within specific temperature ranges (Bossa et al. 2008), and (2) the irradiation of particles by UV photons (Bossa et al. 2008; Tenelanda-Osorio et al. 2022).

Section 2 details the CPD model and the framework for simulating particle transport used in this study. It also explains how the thermodynamic conditions necessary for COM formation via thermal processing and irradiation are incorporated into the model. Section 3 presents the resulting COM formation pathways within the evolving CPD environment. Finally, Section 4 explores how sensitive our results are to a larger set of parameters. This section also discusses the broader implications of our findings for satellite formation and the potential for capturing and preserving COMs during this period.

2. MODEL

2.1. Jovian Circumplanetary Disk

The CPD model used in this study is axisymmetric and assumes hydrostatic equilibrium. We adopt the two-dimensional framework presented by Schneeberger & Mousis (2024), which builds upon the models developed by Makalkin & Dorofeeva (2014) and Heller & Pudritz (2015). This framework incorporates the viscous accretion disk prescription from Canup & Ward (2002). The outer boundary of the CPD is assumed to be located at $133 R_{\text{Jup}}$, which corresponds to one-fifth of Jupiter's Hill radius. The temperature and density profiles within the CPD are governed by its time-dependent accretion rate, which is parameterized following the formulation of Sasaki et al. (2010):

$$\dot{M}(t) = \dot{M}_0 \exp\left(-\frac{t}{\tau}\right) M_{\text{J}}/\text{yr}, \quad (1)$$

where $\dot{M}(t)$ represents the disk accretion rate at time t , and \dot{M}_0 corresponds to the accretion rate at the end of Jupiter's gas runaway accretion phase, when the planet reached 95% of its current mass. The variable τ is the characteristic depletion timescale of the CPD, estimated to range from 20 kyr to 1 Myr (Sasaki et al. 2010; Mordasini 2013). Additionally, the CPD's thermodynamic conditions are influenced by Jupiter's mass, radius, and surface temperature. In our model, Jupiter's mass is fixed at 95% of its present value, while its radius is assumed to be 10% larger, reflecting the planet's inflated state and elevated surface temperature of approximately 2000 K (Mordasini 2013).

The properties of the CPD also depend on the viscosity ν , which is expressed as

$$\nu(r, z) = \alpha \frac{C_s^2(r, z)}{\Omega_K(r)}, \quad (2)$$

where $C_s(r, z)$ is the speed of sound at a given planet-centered radius, r , and height, z , above the disk midplane. $\Omega_K(r)$ represents the Keplerian angular frequency at radius r from the planet. The constant α , which typically ranges from 10^{-4} to 10^{-2} , scales the strength of the viscosity in the CPD. This parameter is constrained by both observations and theoretical models of protoplanetary disks (Shakura & Sunyaev 1973; Lynden-Bell & Pringle 1974; Villenave et al. 2022).

The structure of the CPD also depends on the location of its centrifugal radius, R_c . Within this radius, the CPD's gas drifts inward toward the planet, while beyond this radius it flows outward, merging with the meridional flow within the planet's Hill Sphere (Tanigawa et al. 2012; Morbidelli et al. 2014; Szulágyi et al. 2014). In gas-starved CPD models, R_c is typically assumed to be farther than the present location of Callisto, which is at $26.9 R_{\text{Jup}}$ from Jupiter (Sasaki et al. 2010).

The material forming the CPD is accreted from the protoplanetary disk, which has an average molecular mass μ_g of $2.341 \times 10^{-3} \text{ kg.mol}^{-1}$ (Aguichine et al. 2022) and a metallicity of $\frac{Z}{H} = 2.45 \times 10^{-2}$ (Lodders 2019). However, simulations suggest that the CPD can only accrete dust located at high altitudes within the PPD. Therefore, we assume that the dust-to-gas ratio in the accreted material is only one tenth of that in the protoplanetary disk (Lambrechts & Johansen 2012; Zhu et al. 2012). In the CPD model this results in a metallicity of 2.45×10^{-3} .

Figure 1 shows the temperature and pressure profiles of a CPD model, assuming $\dot{M}_0 = 6.6 \times 10^{-6} M_{\text{Jup}} \cdot \text{yr}^{-1}$,

$\tau = 2 \times 10^4 \text{ yr}$, $\alpha = 10^{-3}$, and $R_c = 50 R_{\text{Jup}}$, as derived by Mordasini (2013). This set of parameters constitutes our nominal model in the following analysis. The figure highlights a peculiar feature of the model: radiative transfer calculations produce "shadows" that locally cool the CPD down to 100 K below the ambient gas temperature. With this set of parameters, the disk has a short lifetime, depleting in less than 200 kyr, and transitions from being massive and hot to cold and light. This particular choice of parameters accounts for the rapid opening of a gap within the PPD at Jupiter's location, which halts the accretion of matter (Mordasini 2013).

2.2. Transport of particles

We use a particle transport model based on Ciesla (2010, 2011) and Benest Couzinou et al. (2024), which calculates the radial and vertical evolution of individual particles in a protoplanetary disk following a Lagrangian approach. We adapted this model to the CPD environment. The vertical evolution of particles is based on the following advection diffusion equation (Dubrulle et al. 1995; Gail 2001; Ciesla 2010):

$$\frac{\partial \rho_s}{\partial t} = \frac{\partial}{\partial z} \left(\rho_g D \frac{\partial \rho_g}{\partial z} \right) - \frac{\partial}{\partial z} (\rho_s v_z), \quad (3)$$

which depends on the density of the material ρ_s , the density of the gas ρ_g , the diffusivity $D = \frac{\nu}{1+St^2}$, the Stokes number St , and the terminal velocity of the particles v_z (Cuzzi & Weidenschilling 2006; Ciesla 2010). The radial evolution of the particles is analogous to this expression, but along the x and y cartesian axes. The vertical velocity $v_{\text{eff},z}$ derived from this expression is used to compute the vertical position of the particles (Ciesla 2010):

$$z_i = z_{i-1} + v_{\text{eff},z} \delta t + R_1 \left[\frac{2}{\sigma^2} D(z) \delta t \right]^{\frac{1}{2}}. \quad (4)$$

This expression computes the vertical position z_i after a time step $\delta t = 1/\Omega_K$, given an initial vertical position z_{i-1} . The random motion induced by the gas turbulence is parameterized by the random number $R_1 \in [-1; 1]$ and its distribution variance σ^2 ($= 1/3$ for a uniform distribution, Visser (1997)). $v_{\text{eff},z}$ is the vertical velocity of the particle and the sum of the following three terms (Ciesla 2010):

$$v_{\text{eff},z} = v_z + \frac{D}{\rho_g} \frac{\partial \rho_g}{\partial z} + \frac{\partial D}{\partial z}, \quad (5)$$

where $v_z = -t_s \Omega_K^2 z$ is the terminal velocity. The second term considers the vertical gradient of the density in the disk, and the last term considers the vertical variation

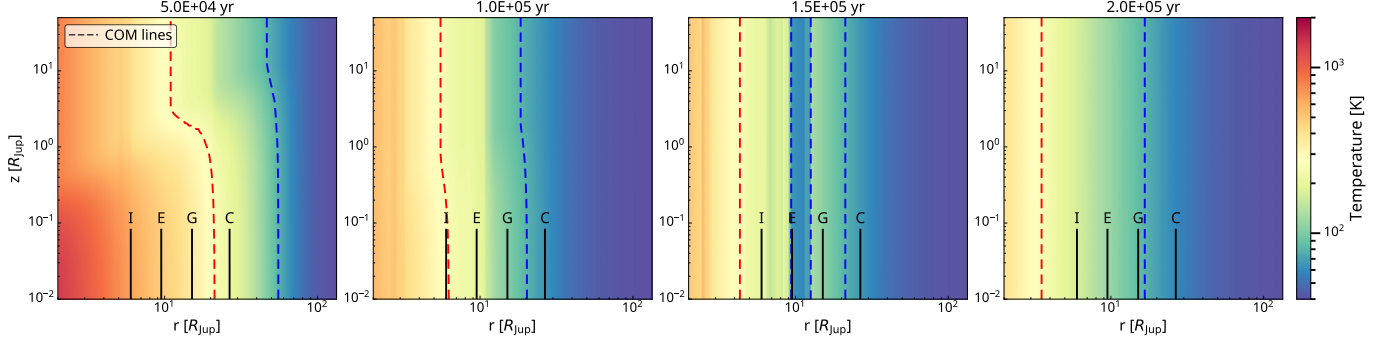


Figure 1. Temperature profiles of the CPD at $t = 50, 100, 150$, and 200 kyr of its evolution. The formation of COMs by thermal processing occurs in the temperature range from 80 K (blue dashed line) to 260 K (red dashed line). At 150 kyr of evolution, a cold region appears in the model, with temperatures too low to support COM formation by thermal processing.

of the diffusion coefficient (Ciesla 2010; Ronnet et al. 2017; Benest Couzinou et al. 2024). The stopping time t_s is calculated in the Epstein regime with the following expression (Perets & Murray-Clay 2011; Mousis et al. 2018):

$$t_s = \frac{\rho_s}{\rho_g} \frac{R_s}{v_{\text{th}}}, \quad (6)$$

where ρ_g is the density of the gas, R_s is the size of a particle, and $v_{\text{th}} = \sqrt{8/\pi} c_s$ is the thermal velocity.

The radial trajectory of the particles is computed with a similar equation, along the x and y axes (with $r^2 = x^2 + y^2$):

$$x_i = x_{i-1} + v_{\text{eff},x} \delta t + R_1 \left[\frac{2}{\sigma^2} D(r) \delta t \right]^{\frac{1}{2}}, \quad (7)$$

where x_i and x_{i-1} are the horizontal positions of the particle after and before a time step δt , respectively. Because the y -axis equations are the same, due to axisymmetry, only the x -axis equations are described here. The horizontal velocity $v_{\text{eff},x}$ is the sum of three terms (Ciesla 2011):

$$v_{\text{eff},x} = v_r \frac{x_{i-1}}{r_{i-1}} + \frac{D}{\rho_g} \frac{\partial \rho_g}{\partial r} \frac{x_{i-1}}{r_{i-1}} + \frac{\partial D}{\partial r} \frac{x_{i-1}}{r_{i-1}}. \quad (8)$$

Here, the last two terms are similar to those in the vertical velocity equation. The first term v_r is the sum of the velocity of the gas and the radial drift of the particle. It depends on the Stokes number ($\text{St} = t_s \Omega_K$) of the particle, so small particles are less sensitive to radial drift and more coupled to the gas, and vice versa. Its expression is (Birnstiel et al. 2012):

$$v_r = -\frac{1}{1 + \text{St}^2} \frac{\dot{M}}{2\pi \Sigma r} \delta_{r_c} + \frac{2\text{St}}{1 + \text{St}^2} \frac{c_s^2}{r \Omega_K} \frac{d \ln P}{d \ln r}, \quad (9)$$

where δ_{r_c} is a term with a value of 1 if $r > r_c$ and -1 otherwise, and Σ is the surface density in the CPD. It

accounts for the direction of the gas velocity: the gas diffuses outward in regions farther than the centrifugal radius and inward in the inner parts of the CPD.

Figure 2 presents the trajectory of a $100 \mu\text{m}$ particle with a density ρ_s of 1 g.cm^{-3} , released from one scale height ($H = \frac{C_s}{\Omega_K}$, corresponding to $\sim 13.8 R_{\text{Jup}}$) above the CPD midplane at a radial distance of $115 R_{\text{Jup}}$. The particle is introduced at $t_0 = 100$ kyr, which denotes the time elapsed since the formation of the CPD in our nominal model. After its release, the particle reaches Jupiter and stabilizes its vertical motion near the midplane in just over one thousand years.

2.3. COM formation in the Jovian Circumplanetary Disk

In this study, we investigate how two distinct processes, namely irradiation and thermal processing, affect $\text{NH}_3:\text{CO}_2$ and CH_3OH ices carried by particles through the Jovian CPD. Laboratory experiments by Tenelanda-Osorio et al. (2022) show that COM formation in UV-irradiated pure CH_3OH ice depends on UV fluence and temperature, with family-dependent onset behaviors rather than a single sharp threshold. Under far-UV irradiation dominated by Lyman- α photons, several COMs (notably $\text{C}_2\text{--C}_5$ esters and ketones) are already produced at low fluence ($\sim 9 \times 10^{15} \text{ photons cm}^{-2}$ at 20 K), while increasing fluence progressively favors heavier species through radical-radical recombination. The maximum fluence explored, $8.64 \times 10^{17} \text{ photons cm}^{-2}$, corresponds to 24 h of irradiation at a flux of order $10^{13} \text{ photons cm}^{-2} \text{ s}^{-1}$ and marks the upper bound of the laboratory conditions rather than a formation threshold. Similarly, Bossa et al. (2008) demonstrate that $\text{NH}_3:\text{CO}_2$ ices generate COMs under UV irradiation, with a threshold dose of $4.32 \times 10^{19} \text{ photons cm}^{-2}$. These irradiation thresholds are critical parameters in our analysis. Here, the irradiation of ices is modeled as the accumulation of UV radiation within the disk, varying with the particles' position (Benest Couzinou et al.

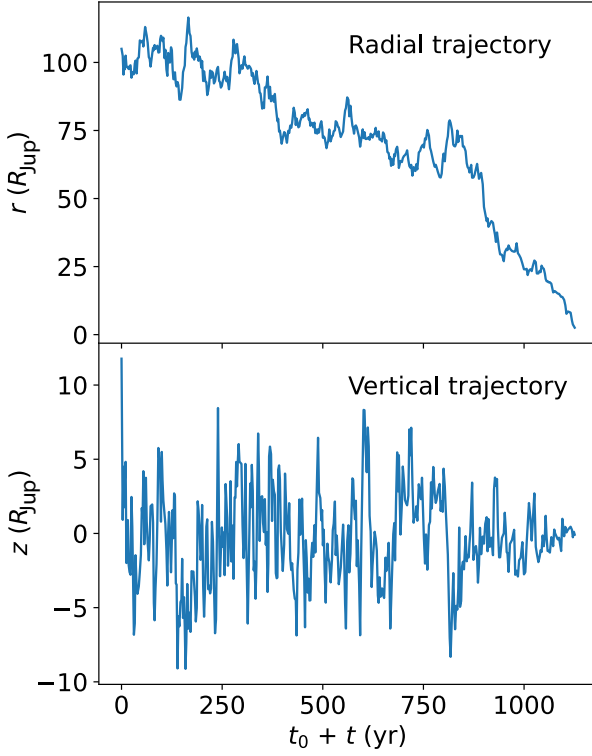


Figure 2. Radial and vertical trajectory of a $100\ \mu\text{m}$ particle released at one scale height above the midplane of the CPD at the distance of $115\ R_{\text{Jup}}$, with an initial release time $t_0 = 100$ kyr, in the case of our nominal model.

2024, 2025). The CPD is exposed to UV interstellar radiation, assumed to be incident perpendicularly to the disk plane. The UV flux, $F(r, z)$, depends on the radial (r) and vertical (z) positions within the disk and is expressed as (Ciesla 2010; Ciesla & Sandford 2012; Benest Couzinou et al. 2024):

$$F(r, z) = F_0 e^{-\tau(r, z)}, \quad (10)$$

where the optical depth, $\tau(r, z)$, is expressed as

$$\tau(r, z) = \int_{|z|}^{\infty} \rho_g(r, z) \kappa \, dz. \quad (11)$$

The initial incident UV flux, F_0 , is set to 10^8 photons $\text{cm}^{-2} \text{s}^{-1}$ (equivalent to $G_0=1$ in Habing units). The opacity, κ , is assumed to correspond to the frequency-averaged mean Rosseland opacity, which is the one used in the underlying CPD model. (Bell & Lin 1994; Aguchine et al. 2020; Schneeberger et al. 2023). It is important to emphasize that, in our simulations, COM formation by irradiation of CH_3OH -bearing grains competes with their sublimation during inward drift in the PSN. We adopt a sublimation temperature of 105 K for CH_3OH , representative of PSN conditions (Mousis et al. 2009). Because these grains are small and porous, we

treat sublimation as effectively instantaneous once this temperature is reached. Consequently, COM formation can only proceed if the grains accumulate the required irradiation dose before they sublimate.

In addition to UV irradiation, Bossa et al. (2008) experimentally find that thermal heating drives the formation of COMs in $\text{NH}_3:\text{CO}_2$ ices at temperatures above 80 K. Specifically, the reactants begin to react at temperatures above 80 K and are completely consumed by 130 K. Two COMs are formed: ammonium carbamate, $[\text{NH}_2\text{COO}^-][\text{NH}_4^+]$ (C), and carbamic acid, NH_2COOH (D), with a 1:1 ratio observed at 140 K. Both species sublimate between 230 and 260 K: C decomposes into CO_2 and NH_3 vapors at 230 K, while D partially decomposes during desorption at 260 K. Consequently, we identify the temperature range of 80–260 K as the zone where COMs form via thermal heating and remain stable within the Jovian CPD.

3. RESULTS

Simulations of particle trajectories have been performed for various particle sizes, disk parameters, and release epochs t_0 during CPD evolution. In all cases, it is assumed that the particles have a uniform density of $1\ \text{g.cm}^{-3}$. Each simulation tracks the trajectories of 800 particles of identical size, released from one scale height above the CPD midplane, and uniformly distributed across 14 release points spaced every $10\ R_{\text{Jup}}$ from 5 to $135\ R_{\text{Jup}}$.

Figure 3 illustrates the time evolution of the median radial trajectories of particles of $1\ \mu\text{m}$, $100\ \mu\text{m}$, $1\ \text{mm}$ and $1\ \text{cm}$ released at $t_0 = 50$ kyr from the 14 different locations in the case of the nominal CPD model. As expected, most particles in the $1\mu\text{m}$ to 1mm size range are strongly coupled to the gas. Those released within the centrifugal radius R_c ($50\ R_{\text{Jup}}$), follow the inward motion of the gas and reach Jupiter in less than 300 years. Conversely, most of the particles originating beyond R_c are carried outward by the gas flow, reaching the outer edge of the CPD over a similar timescale. In contrast, 1cm particles experience significant gas drag and migrate inward more rapidly, reaching Jupiter in just over 100 yr. The particle trajectories also include segments that traverse the thermal processing region of $\text{NH}_3\text{-CO}_2$ ices, leading to the formation of COMs. This region lies between $\sim 20.6\ R_{\text{Jup}}$ and R_c within ~ 300 years after t_0 . If the Galilean moon embryos are still growing in this region after $t_0 = 50$ kyr into the CPD's evolution, they would be able to accrete COM-rich particles.

Figure 3 also presents the average irradiation experienced by particles along their radial trajectories for each batch of particles over time. Here, we consider

only the particles migrating inward within the CPD, as these are more likely to be accreted by the forming Galilean moons. Two irradiation thresholds are indicated: a lower fluence of 8.64×10^{17} photons cm^{-2} inferred from the laboratory experiments of [Tenelanda-Osorio et al. \(2022\)](#), corresponding to the maximum UV dose explored in that study, and a higher fluence of 4.32×10^{19} photons cm^{-2} reported by [Bossa et al. \(2008\)](#). Assuming the particles are primarily composed of CH_3OH ice, none reach the lower threshold, as they sublimate within a few hundred years at temperatures near 105 K ([Mousis et al. 2009](#)), early during their migration through the CPD. If, instead, the particles are composed of an $\text{NH}_3:\text{CO}_2$ ice mixture, the figure shows that thermal processing would convert the ice into COMs well before the irradiation threshold is reached. These results suggest that, under these compositional assumptions, thermal processing is the dominant pathway for COM formation in the CPD.

The parameters adopted in Figs. 4 and 5 are identical to those used in Fig. 3, except that particles are released at $t_0 = 100$ kyr and $t_0 = 150$ kyr, respectively, during the evolution of the CPD. Since these release epochs occur later, the gas density in the CPD has decreased compared to the conditions at $t_0 = 50$ kyr. As the gas density decreases, the Stokes number of the particles increases, since it is inversely proportional to the local gas density ($\text{St} \propto 1/\rho_{\text{gas}}$). This increase in the Stokes number results in weaker coupling between the particles and the gas. Consequently, at $t_0 = 100$ kyr, particles with sizes exceeding $100 \mu\text{m}$ are predominantly subject to gas drag, whereas at $t_0 = 150$ kyr, even particles as small as $1 \mu\text{m}$ exhibit inward drift, experiencing gas drag effects beyond R_c . At $t_0 = 100$ kyr and 150 kyr, the thermal processing region shifts closer to Jupiter within the CPD, lying within approximately $\sim 20 R_{\text{Jup}}$ during these stages of the disk's evolution. Ices composed of $\text{NH}_3:\text{CO}_2$, whether carried by grains influenced by gas drag or by the smallest particles tightly coupled to the gas and released below R_c , transit through this region. During this passage, thermal processing may convert these ices into COMs.

Interestingly, Fig. 4 indicates that particles released at $t_0 = 100$ kyr beyond approximately 75 and $125 R_{\text{Jup}}$, with sizes of $1 \mu\text{m}$ and $100 \mu\text{m}$, respectively, follow trajectories that exceed the irradiation threshold defined by [Tenelanda-Osorio et al. \(2022\)](#). However, as the figure shows, most of these particles lose their CH_3OH ice due to sublimation before reaching this threshold. A similar trend is observed in Fig. 5, where the computed trajectories of $1\text{-}\mu\text{m}$ particles released at $t_0 = 150$ kyr beyond approximately $85 R_{\text{Jup}}$ in the CPD reach the irradiation

threshold, while most of them have lost their CH_3OH ice by that time.

Figure 6 shows the distribution of residence times for particles within the COM thermal stability region, considering particles of sizes $1 \mu\text{m}$ and 1 cm , released into the CPD at $t_0 = 50, 100$, and 150 kyr after its formation. Both particle sizes have short residence times, with the largest particles being removed fastest. For $1 \mu\text{m}$ particles, the residence time distribution peaks at around 100 yr at $t_0 = 50$ kyr and shifts to approximately 200 yr at $t_0 = 100$ and 150 kyr. In contrast, 1 cm particles exhibit much shorter residence times. Those released at $t_0 = 50$ kyr typically remain within the thermal stability region of COMs for less than 30 yr, decreasing to under 4 yr at $t_0 = 100$ kyr. None of the 1 cm particles released at $t_0 = 150$ kyr remain in the stability region for more than 1 yr, which corresponds to the temporal resolution of the iterative scheme of our model.

4. DISCUSSION

Overall, our simulations suggest that particles of varying sizes, released at different points during the evolution of the CPD, pass through regions where temperatures are high enough to thermally process ices, particularly $\text{NH}_3:\text{CO}_2$ ices, into complex COMs. This transformation occurs before significant irradiation, indicating that thermal processes, rather than photochemical reactions, primarily drive the formation of COMs in this environment. Furthermore, particles typically reach the methanol iceline before they can absorb a sufficient number of photons, making the formation of COMs through irradiation a challenging and intricate process in CPDs.

The results of our study have been tested across a large range of parameter sets. For instance, an increase in particle density leads to a faster inward drift. Specifically, all 1 cm particles with a density of 3 g.cm^{-3} reach Jupiter in less than 40 yr, compared to ~ 100 yr for particles with a density of 1 g.cm^{-3} , assuming $t_0 = 50$ kyr. This indicates that the formation of COMs via irradiation is more challenging, as these particles receive lower irradiation doses. Nevertheless, they still traverse the thermal processing zone. Reducing the value of R_c , for instance to $17 R_{\text{Jup}}$, has little effect on the irradiation doses received by the smallest particles. However, it reduces the efficiency of COM formation via thermal processing. As R_c moves closer to Jupiter, fewer small particles are entrained in the inward gas flow and transported through the thermal processing region. In contrast, the dynamics of larger particles, which are primarily governed by gas drag, remain largely unaffected by variations in R_c in terms of both irradiation and thermal processing.

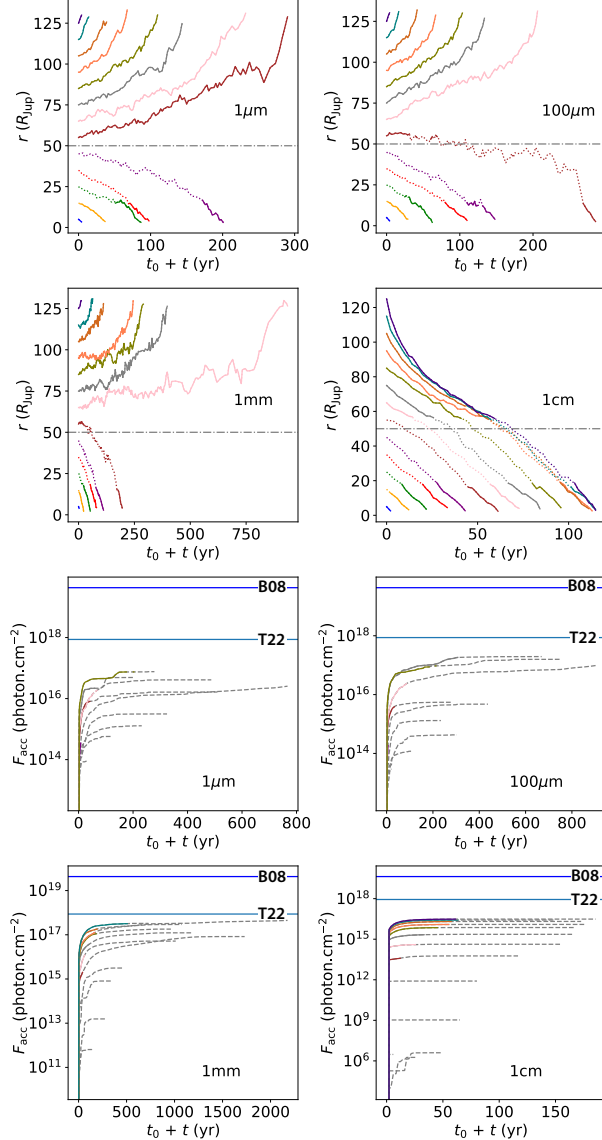


Figure 3. *Top four panels:* median radial trajectories of $1\mu\text{m}$, $100\mu\text{m}$, 1mm , and 1cm particles as a function of time in our nominal CPD model. The particles are released one scale height above the CPD midplane at $t_0 = 50$ kyr. Median trajectories are shown at $10 R_{\text{Jup}}$ intervals in the midplane, spanning from 5 to $135 R_{\text{Jup}}$ in the CPD. Dotted lines highlight portions of these trajectories that intersect the COM formation zone via thermal processing in the CPD. The horizontal dotted-dashed line indicates the location of R_c . *Bottom four panels:* average irradiation experienced by particles migrating inward within the CPD, shown as a function of time in the nominal CPD model. The two horizontal lines represent the irradiation thresholds discussed in the text, while the dashed curves indicate the fraction of trajectories where CH_3OH is in the vapor phase. T22 and B08 refer to the irradiation thresholds experimentally derived by Tenelanda-Osorio et al. (2022) and Bossa et al. (2008), respectively.

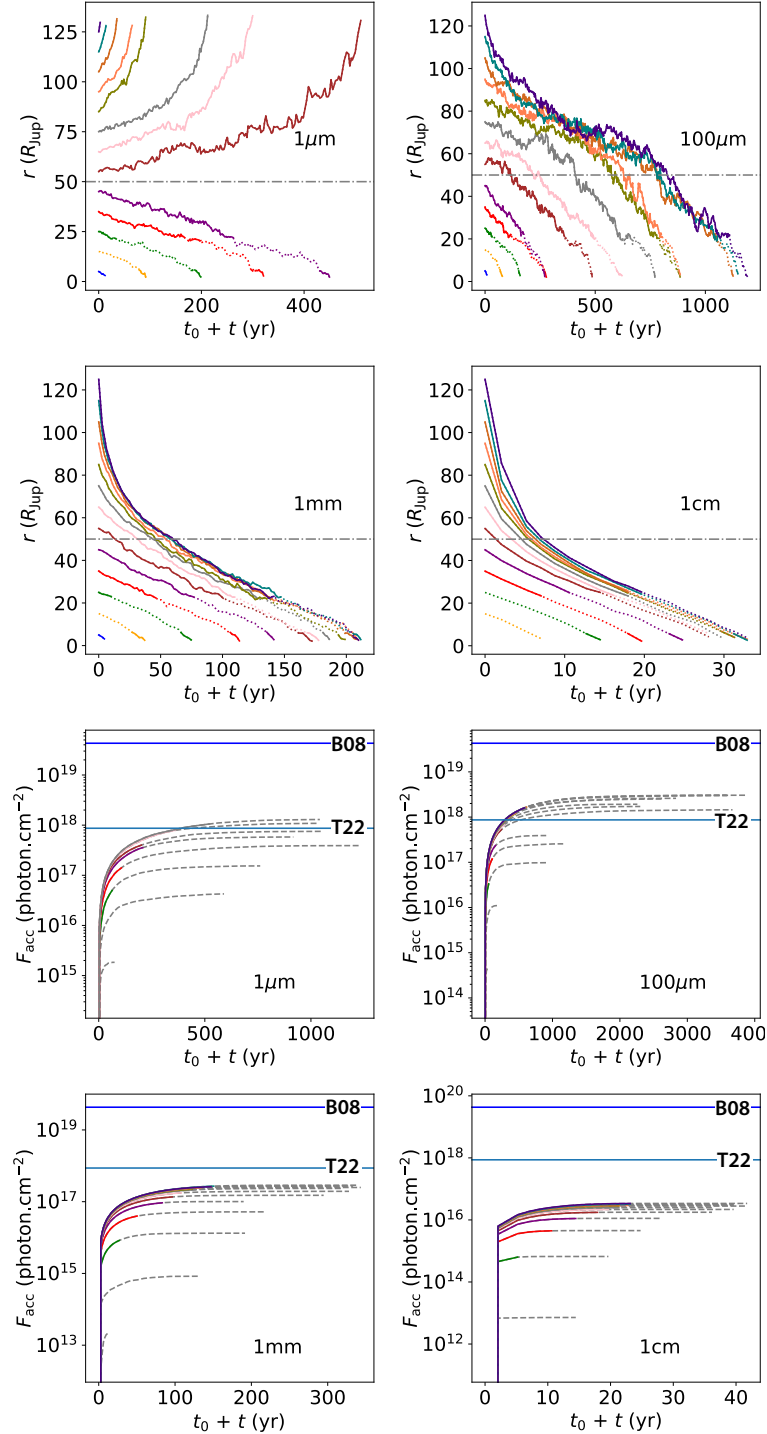


Figure 4. Same as Fig. 3, but with particles released at $t_0 = 100$ kyr.

An increase in the turbulent viscosity parameter, α , of the CPD results in a lower surface density and a lower midplane temperature. This limits the spatial extent of regions where thermal processing of particles can occur at a given stage of the CPD’s evolution. Furthermore, increasing α reduces the likelihood of COM formation

by irradiation. For example, when $\alpha = 10^{-2}$, COMs are not produced by irradiation because the lower gas density increases the Stokes number of small particles, which weakens their coupling to the gas. Consequently, these particles drift inward more rapidly toward Jupiter, shortening their residence time in the outer CPD where

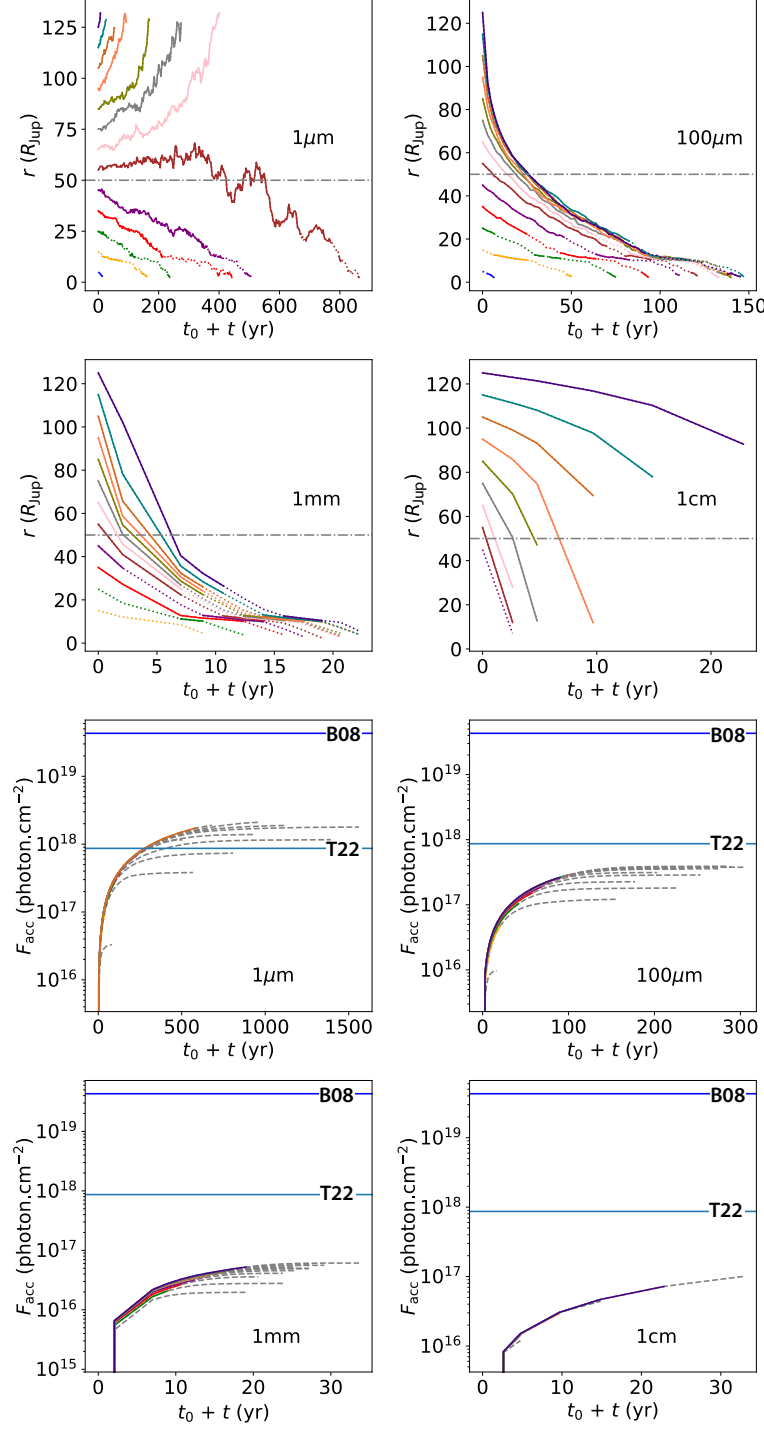


Figure 5. Same as Fig. 3, but with particles released at $t_0 = 150$ kyr.

irradiation is effective. Decreasing the CPD accretion rate has a similar effect to increasing the turbulent viscosity parameter, α , resulting in lower surface densities and midplane temperatures. Decreasing the CPD's accretion rate by an order of magnitude, for instance, reduces the particles' residence time within the disk by

about half, thereby limiting their exposure to conditions conducive to COM formation via irradiation.

The limited availability of laboratory photochemical data introduces unavoidable uncertainties in our modeling. Our approach relies on the most recent UV-irradiation experiments, which probe a relatively narrow

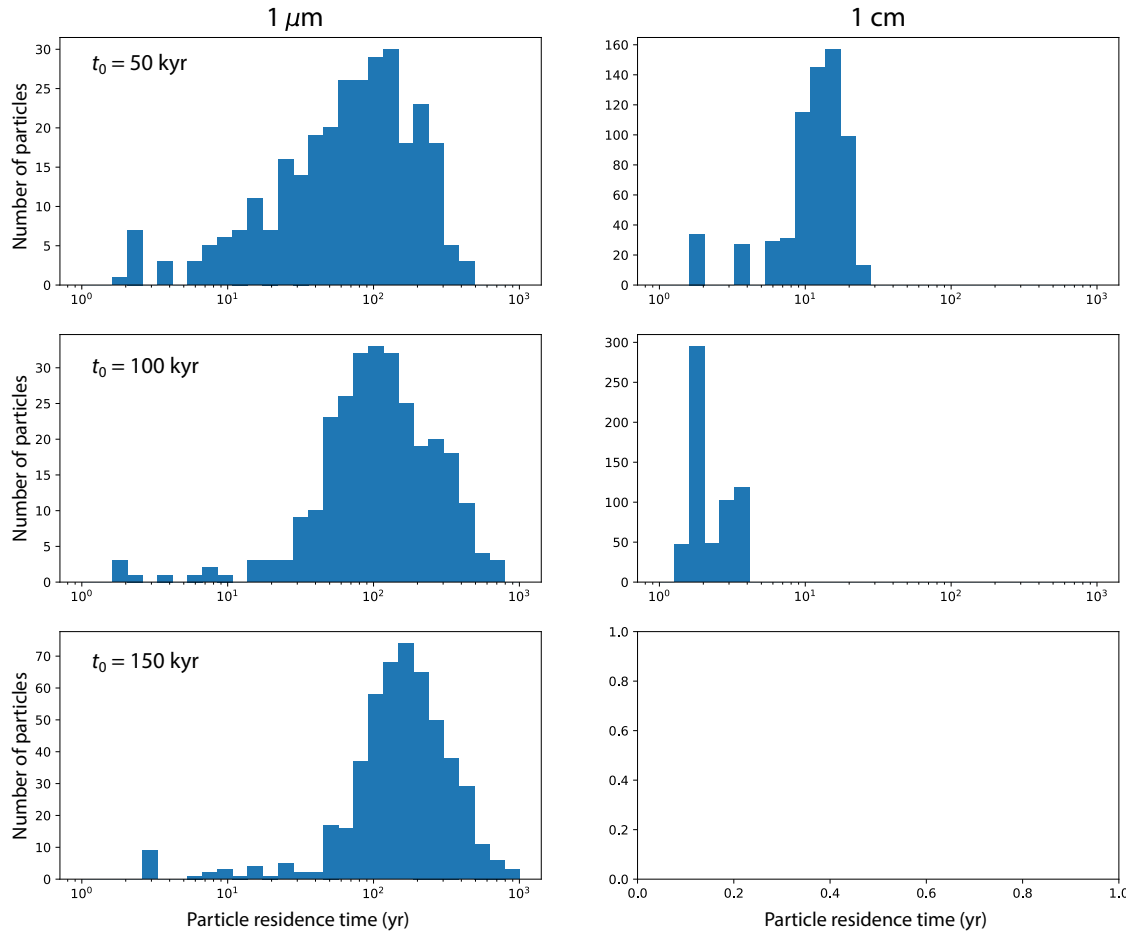


Figure 6. Time evolution of the number of $1\text{ }\mu\text{m}$ and 1 cm particles remaining in the COM stability region ($\sim 80\text{--}260\text{ K}$), relative to an initial set of 800 particles released in our nominal CPD model. From top to bottom, the particles were initially uniformly distributed between 5 and $135\text{ }R_{\text{Jup}}$ at one scale height above the CPD midplane, with starting epochs $t_0 = 50, 100$, and 150 kyr , respectively. When $t_0 \simeq 150\text{ kyr}$, 1 cm particles migrate on timescales shorter than the adopted CPD evolution timestep (1 yr).

wavelength range and may therefore bias the predicted reaction pathways and yields of COMs. Consistent with previous studies adopting similar formalisms to evaluate irradiation in PPDs (Muñoz Caro et al. 2002; Öberg et al. 2009; Benest Couzinou et al. 2024, 2025), our chemical model includes only a restricted set of formation and destruction processes and neglects hydrogenation reactions (Linnartz et al. 2011), as well as secondary UV photons generated by cosmic-ray interactions with H_2 gas (Prasad & Tarafdar 1983). Reactions involving additional molecular species and the implementation of more comprehensive photochemical networks (Takehara et al. 2022; Ochiai et al. 2024) are also not considered, which may limit the model’s ability to fully capture the chemical evolution within the CPD.

It is worth noting that, thermal and photochemical processes operate through fundamentally different mechanisms: thermal reactions primarily drive molecular reorganization in warm regions, whereas photochem-

istry dominates in UV-irradiated layers. Future laboratory studies spanning a broader range of photon energies and irradiation conditions will be essential to further refine chemical models and improve quantitative predictions. Nevertheless, we expect our main qualitative conclusions to remain robust, as they are governed by the distinct roles of thermal and photochemical processing rather than by the precise efficiencies of individual reaction pathways.

The present study intentionally isolates the chemical evolution of COMs, whereas in astrophysical environments these species coexist with water ice, silicates, and carbonaceous grains that can significantly influence their stability and reactivity. When CH_3OH is embedded in an H_2O -rich matrix, UV irradiation of the ice substantially modifies both radical production and subsequent chemical evolution (Öberg et al. 2010). Increasing the H_2O fraction enhances the photodestruction efficiency of volatile constituents and shifts the product distri-

bution toward more oxygen-rich species while simultaneously promoting radical trapping in the ice matrix and disproportionately inhibiting OH diffusion relative to CH₃ and HCO. These competing effects imply that, although H₂O-rich ices can efficiently generate radicals, the formation pathways and yields of complex organic molecules are strongly regulated by mixture-dependent radical mobility, emphasizing the need to account for H₂O-controlled diffusion and trapping when interpreting or modeling COM formation in astrophysical ices.

Adsorption onto mineral and carbonaceous surfaces can also modify reaction barriers and promote catalytic organic processing (Herbst & van Dishoeck 2009; Minissale et al. 2016; Cuppen et al. 2017), while incorporation within mixed ice–dust aggregates can reduce the effective UV flux reaching embedded molecules through geometric and optical shielding, thereby limiting UV photodissociation (Potapov et al. 2020) and affect their retention and release during thermal desorption and sublimation (Fayolle et al. 2011). Future work will explore the inclusion of simplified adsorption–desorption processes in the photochemical–thermal framework to examine their potential influence on the survival and distribution of COMs in the Jovian CPD.

Although the total irradiation dose was compared with laboratory conditions, the significantly lower irradiation rate in the CPD likely limits molecular complexity, as radicals formed under such conditions have more time to recombine into their precursors. Second, the treatment of opacity and UV irradiation introduces additional limitations. In particular, the Rosseland mean opacity adopted in the CPD model, being frequency-averaged, does not adequately represent UV-specific processes, as already noted in the context of PPDs (Bennest Couzinou et al. 2024). Although this limitation could lead to an underestimation of UV penetration and thus of irradiation-driven chemistry, it is partially compensated by the assumption that the adopted interstellar UV flux, F_0 , represents a lower bound. Higher irradiation levels are plausible during the early evolution of the Solar System, especially during the CPD phase. Such elevated fluxes could significantly enhance the formation of COMs via irradiation-driven processes. A likely scenario for achieving high UV fluxes involves the formation of the Sun within a dense stellar cluster, in close proximity (≤ 0.03 –0.05 pc) to one or more O-type stars. These stars emit intense FUV radiation, capable of generating flux levels as high as $G_0 = 30,000$ (Adams et al. 2004; Fatuzzo & Adams 2008). Additionally, meteoritic evidence, including the presence of short-lived radionuclides such as ²⁶Al and ⁶⁰Fe, suggests that the early solar system experienced significant external irra-

diation, possibly from nearby supernovae (Lichtenberg et al. 2016). These extreme, yet observationally supported conditions, are consistent with a clustered origin for the Sun.

Our calculations suggest that, if COM-rich particles were present in the CPD, either formed in situ or delivered from the PPD, the Galilean moons could have incorporated these materials during their accretion. However, accounting for their present-day physical states implies that each moon must have formed under distinct conditions, leading to varying efficiencies in retaining solid-phase COMs within their interiors. The thermal environment during accretion was likely influenced by multiple factors, including the sizes of the moons and their impactors, the local disk temperature, and the duration of the accretion process (Canup & Ward 2002; Bierson & Nimmo 2020; Bennacer et al. 2025).

The combination of accretional heating and high ambient temperatures in the inner CPD may have led to high-temperature accretion of Io and Europa (Bierson & Nimmo 2020), causing the destruction of COMs. However, more recent studies suggest that Europa may have formed under cooler conditions (Trinh et al. 2023; Petricca et al. 2025), where the gravitational energy delivered by impactors was minor compared to the background thermal input from the CPD, due to a prolonged accretion period (Canup & Ward 2002). In this context, assuming a low heat dissipation efficiency ($h \sim 0.01$), the Europa accretion temperature would closely follow the local CPD temperature, estimated between 200 and 300 K at its formation site. Thus, COMs could have remained stable within Europa if it accreted slowly, typically over several million years, and at a distance greater from Jupiter than its current orbit.

Both Ganymede and Callisto are thought to have formed beyond the snow line in the colder regions of the CPD. Depending on the size distribution of the impactors and the duration of accretion, Ganymede’s accretional history could have been warm or cold (Barr & Canup 2008; Bierson & Nimmo 2020; Bjonnes et al. 2022; Bennacer et al. 2025). Bennacer et al. (2025) recently showed that Ganymede could avoid global melting only if it accreted slowly and primarily from small particles with radii $r_{\text{imp}} \lesssim 100$ m. Even in scenarios involving a substantial fraction of kilometer-sized impactors, thermal models indicate that elevated temperatures would largely be confined to the final stages of accretion. This suggests that Ganymede may have retained a significant fraction of its primordial COMs. Callisto, by contrast, is widely believed to have formed under cold accretion conditions, consistent with its partially differentiated interior and incomplete ice–rock seg-

regation (Anderson et al. 2001; Barr & Canup 2008; Bennacer et al. 2025). Consequently, both moons may have

retained substantial fractions of the COMs acquired during their formation.

REFERENCES

Adams, F. C., Hollenbach, D., Laughlin, G., & Gorti, U. 2004, *ApJ*, 611, 360, doi: [10.1086/421989](https://doi.org/10.1086/421989)

Aguichine, A., Mousis, O., Devouard, B., & Ronnet, T. 2020, *The Astrophysical Journal*, 901, 97, doi: [10.3847/1538-4357/abaf47](https://doi.org/10.3847/1538-4357/abaf47)

Aguichine, A., Mousis, O., & Lunine, J. I. 2022, *The Planetary Science Journal*, 3, 141, doi: [10.3847/PSJ/ac6bf1](https://doi.org/10.3847/PSJ/ac6bf1)

Anderson, J., Jacobson, R., McElrath, T., et al. 2001, *Icarus*, 153, 157, doi: <https://doi.org/10.1006/icar.2001.6664>

Anderson, S. E., Mousis, O., & Ronnet, T. 2021, *The Planetary Science Journal*, 2, 50, doi: [10.3847/PSJ/abe0ba](https://doi.org/10.3847/PSJ/abe0ba)

Barr, A., & Canup, R. 2008, *Icarus*, 198, 163

Becker, T. M., Zolotov, M. Y., Gudipati, M. S., et al. 2024, *SSRv*, 220, 49, doi: [10.1007/s11214-024-01069-y](https://doi.org/10.1007/s11214-024-01069-y)

Bell, K. R., & Lin, D. N. C. 1994, *The Astrophysical Journal*, 427, 987, doi: [10.1086/174206](https://doi.org/10.1086/174206)

Benest Couzinou, T., Amsler Moulanier, A., & Mousis, O. 2025, in EGU General Assembly Conference Abstracts, EGU General Assembly Conference Abstracts, 5889, doi: [10.5194/egusphere-egu24-5889](https://doi.org/10.5194/egusphere-egu24-5889)

Benest Couzinou, T., Mousis, O., Danger, G., et al. 2024, *A&A*, 692, A10, doi: [10.1051/0004-6361/202449499](https://doi.org/10.1051/0004-6361/202449499)

Bennacer, Y., Mousis, O., Monnereau, M., Hue, V., & Schneeberger, A. 2025, arXiv e-prints, arXiv:2505.07785, doi: [10.48550/arXiv.2505.07785](https://doi.org/10.48550/arXiv.2505.07785)

Bierson, C. J., & Nimmo, F. 2020, *The Astrophysical Journal Letters*, 897, L43, doi: [10.3847/2041-8213/aba11a](https://doi.org/10.3847/2041-8213/aba11a)

Birnstiel, T., Klahr, H., & Ercolano, B. 2012, *Astronomy and Astrophysics*, 539, A148, doi: [10.1051/0004-6361/201118136](https://doi.org/10.1051/0004-6361/201118136)

Bjonne, E., Johnson, B. C., Silber, E. A., Singer, K. N., & Evans, A. J. 2022, *Journal of Geophysical Research (Planets)*, 127, e07028, doi: [10.1029/2021JE007028](https://doi.org/10.1029/2021JE007028)

Bossa, J. B., Theulé, P., Duvernay, F., Borget, F., & Chiavassa, T. 2008, *Astronomy & Astrophysics*, 492, 719, doi: [10.1051/0004-6361:200810536](https://doi.org/10.1051/0004-6361:200810536)

Canup, R. M., & Ward, W. R. 2002, *The Astronomical Journal*, 124, 3404, doi: [10.1086/344684](https://doi.org/10.1086/344684)

—. 2006, *Nature*, 441, 834, doi: [10.1038/nature04860](https://doi.org/10.1038/nature04860)

Ciesla, F. J. 2010, *ApJ*, 723, 514, doi: [10.1088/0004-637X/723/1/514](https://doi.org/10.1088/0004-637X/723/1/514)

—. 2011, *ApJ*, 740, 9, doi: [10.1088/0004-637X/740/1/9](https://doi.org/10.1088/0004-637X/740/1/9)

Ciesla, F. J., & Sandford, S. A. 2012, *Science*, 336, 452, doi: [10.1126/science.1217291](https://doi.org/10.1126/science.1217291)

Couzinou, T. B., Moulanier, A. A., & Mousis, O. 2025, *MNRAS*, doi: [10.1093/mnras/staf2074](https://doi.org/10.1093/mnras/staf2074)

Cuppen, H. M., Walsh, C., Lamberts, T., et al. 2017, *SSRv*, 212, 1, doi: [10.1007/s11214-016-0319-3](https://doi.org/10.1007/s11214-016-0319-3)

Cuzzi, J. N., & Weidenschilling, S. J. 2006, *Particle-Gas Dynamics and Primary Accretion*, 353, <https://ui.adsabs.harvard.edu/abs/2006mess.book..353C>

Dubrulle, B., Morfill, G., & Sterzik, M. 1995, *Icarus*, 114, 237–246, doi: [10.1006/icar.1995.1058](https://doi.org/10.1006/icar.1995.1058)

Fatuzzo, M., & Adams, F. C. 2008, *ApJ*, 675, 1361, doi: [10.1086/527469](https://doi.org/10.1086/527469)

Fayolle, E. C., Öberg, K. I., Cuppen, H. M., Visser, R., & Linnartz, H. 2011, *A&A*, 529, A74, doi: [10.1051/0004-6361/201016121](https://doi.org/10.1051/0004-6361/201016121)

Gail, H. P. 2001, *Astronomy and Astrophysics*, 378, 192–213, doi: [10.1051/0004-6361:20011130](https://doi.org/10.1051/0004-6361:20011130)

Grasset, O., Dougherty, M. K., Coustenis, A., et al. 2013, *Planet. Space Sci.*, 78, 1, doi: [10.1016/j.pss.2012.12.002](https://doi.org/10.1016/j.pss.2012.12.002)

Hand, K. P., Chyba, C. F., Priscu, J. C., Carlson, R. W., & Nealson, K. H. 2009, in *Europa*, ed. R. T. Pappalardo, W. B. McKinnon, & K. K. Khurana, 589

Hartogh, P. 2023, in *AAS/Division for Planetary Sciences Meeting Abstracts*, Vol. 55, AAS/Division for Planetary Sciences Meeting Abstracts #55, 201.02

Heller, R., & Pudritz, R. 2015, *ApJ*, 806, 181, doi: [10.1088/0004-637X/806/2/181](https://doi.org/10.1088/0004-637X/806/2/181)

Herbst, E., & van Dishoeck, E. F. 2009, *ARA&A*, 47, 427, doi: [10.1146/annurev-astro-082708-101654](https://doi.org/10.1146/annurev-astro-082708-101654)

Kivelson, M. G., Khurana, K. K., Russell, C. T., et al. 2000, *Science*, 289, 1340, doi: [10.1126/science.289.5483.1340](https://doi.org/10.1126/science.289.5483.1340)

Lambrechts, M., & Johansen, A. 2012, *A&A*, 544, A32, doi: [10.1051/0004-6361/201219127](https://doi.org/10.1051/0004-6361/201219127)

Lichtenberg, T., Parker, R. J., & Meyer, M. R. 2016, *MNRAS*, 462, 3979, doi: [10.1093/mnras/stw1929](https://doi.org/10.1093/mnras/stw1929)

Linnartz, H., Bossa, J.-B., Bouwman, J., et al. 2011, in *IAU Symposium*, Vol. 280, *The Molecular Universe*, ed. J. Cernicharo & R. Bachiller, 390–404, doi: [10.1017/S1743921311025142](https://doi.org/10.1017/S1743921311025142)

Lodders, K. 2019, *Oxford Research Encyclopedia of Planetary Science*, <https://api.semanticscholar.org/CorpusID:208527688>

Lynden-Bell, D., & Pringle, J. E. 1974, Monthly Notices of the Royal Astronomical Society, 168, 603, doi: [10.1093/mnras/168.3.603](https://doi.org/10.1093/mnras/168.3.603)

Makalkin, A. B., & Dorofeeva, V. A. 2014, Solar System Research, 48, 62, doi: [10.1134/S0038094614010067](https://doi.org/10.1134/S0038094614010067)

McKay, C. P., Porco Carolyn C., Altheide, T., Davis, W. L., & Kral, T. A. 2008, Astrobiology, 8, 909, doi: [10.1089/ast.2008.0265](https://doi.org/10.1089/ast.2008.0265)

Minissale, M., Dulieu, F., Cazaux, S., & Hocuk, S. 2016, A&A, 585, A24, doi: [10.1051/0004-6361/201525981](https://doi.org/10.1051/0004-6361/201525981)

Morbidelli, A., Szulágyi, J., Crida, A., et al. 2014, Icarus, 232, 266, doi: [10.1016/j.icarus.2014.01.010](https://doi.org/10.1016/j.icarus.2014.01.010)

Mordasini, C. 2013, Astronomy & Astrophysics, 558, A113, doi: [10.1051/0004-6361/201321617](https://doi.org/10.1051/0004-6361/201321617)

Mousis, O., Marboeuf, U., Lunine, J. I., et al. 2009, ApJ, 696, 1348, doi: [10.1088/0004-637X/696/2/1348](https://doi.org/10.1088/0004-637X/696/2/1348)

Mousis, O., Ronnet, T., Lunine, J. I., et al. 2018, The Astrophysical Journal, 858, 66, doi: [10.3847/1538-4357/aab6b9](https://doi.org/10.3847/1538-4357/aab6b9)

Muñoz Caro, G. M., Meierhenrich, U. J., Schutte, W. A., et al. 2002, Nature, 416, 403, doi: [10.1038/416403a](https://doi.org/10.1038/416403a)

Öberg, K. I., Garrod, R. T., van Dishoeck, E. F., & Linnartz, H. 2009, A&A, 504, 891, doi: [10.1051/0004-6361/200912559](https://doi.org/10.1051/0004-6361/200912559)

Öberg, K. I., van Dishoeck, E. F., Linnartz, H., & Andersson, S. 2010, ApJ, 718, 832, doi: [10.1088/0004-637X/718/2/832](https://doi.org/10.1088/0004-637X/718/2/832)

Ochiai, Y., Ida, S., & Shoji, D. 2024, A&A, 687, A232, doi: [10.1051/0004-6361/202449655](https://doi.org/10.1051/0004-6361/202449655)

Pappalardo, R. T., Buratti, B. J., Korth, H., et al. 2024, SSRv, 220, 40, doi: [10.1007/s11214-024-01070-5](https://doi.org/10.1007/s11214-024-01070-5)

Perets, H. B., & Murray-Clay, R. A. 2011, The Astrophysical Journal, 733, 56, doi: [10.1088/0004-637X/733/1/56](https://doi.org/10.1088/0004-637X/733/1/56)

Petricca, F., Castillo-Rogez, J. C., Genova, A., et al. 2025, Nature Astronomy, 9, 501, doi: [10.1038/s41550-024-02469-4](https://doi.org/10.1038/s41550-024-02469-4)

Potapov, A., Jäger, C., & Henning, T. 2020, PhRvL, 124, 221103, doi: [10.1103/PhysRevLett.124.221103](https://doi.org/10.1103/PhysRevLett.124.221103)

Poulet, F., Piccioni, G., Langevin, Y., et al. 2024, SSRv, 220, 27, doi: [10.1007/s11214-024-01057-2](https://doi.org/10.1007/s11214-024-01057-2)

Prasad, S. S., & Tarafdar, S. P. 1983, ApJ, 267, 603, doi: [10.1086/160896](https://doi.org/10.1086/160896)

Ronnet, T., Mousis, O., & Vernazza, P. 2017, The Astrophysical Journal, 845, 92, doi: [10.3847/1538-4357/aa80e6](https://doi.org/10.3847/1538-4357/aa80e6)

Sasaki, T., Stewart, G. R., & Ida, S. 2010, The Astrophysical Journal, 714, 1052, doi: [10.1088/0004-637X/714/2/1052](https://doi.org/10.1088/0004-637X/714/2/1052)

Saur, J., Duling, S., Roth, L., et al. 2015, Journal of Geophysical Research (Space Physics), 120, 1715, doi: [10.1002/2014JA020778](https://doi.org/10.1002/2014JA020778)

Schneeberger, A., & Mousis, O. 2024, Planet. Sci. J., Submitted

Schneeberger, A., Mousis, O., Aguichine, A., & Lunine, J. I. 2023, Astronomy & Astrophysics, doi: [10.1051/0004-6361/202244670](https://doi.org/10.1051/0004-6361/202244670)

Shakura, N. I., & Sunyaev, R. A. 1973, Astronomy and Astrophysics, 24, 337

Szulágyi, J., Morbidelli, A., Crida, A., & Masset, F. 2014, The Astrophysical Journal, 782, 65, doi: [10.1088/0004-637X/782/2/65](https://doi.org/10.1088/0004-637X/782/2/65)

Takehara, H., Shoji, D., & Ida, S. 2022, A&A, 662, A76, doi: [10.1051/0004-6361/202243212](https://doi.org/10.1051/0004-6361/202243212)

Tanigawa, T., Ohtsuki, K., & Machida, M. N. 2012, The Astrophysical Journal, 747, 47, doi: [10.1088/0004-637X/747/1/47](https://doi.org/10.1088/0004-637X/747/1/47)

Tenelanda-Osorio, L. I., Bouquet, A., Javelle, T., et al. 2022, Monthly Notices of the Royal Astronomical Society, 515, 5009, doi: [10.1093/mnras/stac1932](https://doi.org/10.1093/mnras/stac1932)

Trinh, K. T., Bierson, C. J., & O'Rourke, J. G. 2023, Science Advances, 9, eadf3955, doi: [10.1126/sciadv.adf3955](https://doi.org/10.1126/sciadv.adf3955)

Vance, S. D., Craft, K. L., Shock, E., et al. 2023, SSRv, 219, 81, doi: [10.1007/s11214-023-01025-2](https://doi.org/10.1007/s11214-023-01025-2)

Villenave, M., Stapelfeldt, K. R., Duchêne, G., et al. 2022, The Astrophysical Journal, 930, 11, doi: [10.3847/1538-4357/ac5fae](https://doi.org/10.3847/1538-4357/ac5fae)

Visser, A. 1997, Marine Ecology Progress Series, 158, 275–281, doi: [10.3354/meps158275](https://doi.org/10.3354/meps158275)

Waite, J. H., Burch, J. L., Brockwell, T. G., et al. 2024, SSRv, 220, 30, doi: [10.1007/s11214-024-01061-6](https://doi.org/10.1007/s11214-024-01061-6)

Walsh, C., Millar, T. J., Nomura, H., et al. 2014, A&A, 563, A33, doi: [10.1051/0004-6361/201322446](https://doi.org/10.1051/0004-6361/201322446)

Wurz, P., Meyer, S., Galli, A., et al. 2018, in EGU General Assembly Conference Abstracts, EGU General Assembly Conference Abstracts, 10091

Zhu, Z., Hartmann, L., Nelson, R. P., & Gammie, C. F. 2012, The Astrophysical Journal, 746, 110, doi: [10.1088/0004-637X/746/1/110](https://doi.org/10.1088/0004-637X/746/1/110)